AGU PUBLICATIONS

JGR

Journal of Geophysical Research: Atmospheres

RESEARCH ARTICLE
10.1002/2015JD024525

Key Points:
- Climate models project robust cloud reduction over tropical land
- Land cloud reduction depends on global ocean warming
- Robust positive feedback despite uncertainty in oceanic warming pattern

Supporting Information:
- Supporting Information S1

Correspondence to:
Y. Kamae,
kamae.yoichi.fw@u.tsukuba.ac.jp

Citation:
Kamae, Y., T. Ogura, M. Watanabe, S.-P. Xie, and H. Ueda (2016), Robust cloud feedback over tropical land in a warming climate, *J. Geophys. Res. Atmos.*, *121*, 2593–2609, doi:10.1002/2015JD024525.

Received 18 NOV 2015
Accepted 26 FEB 2016
Accepted article online 8 MAR 2016
Published online 18 MAR 2016

Robust cloud feedback over tropical land in a warming climate

Youichi Kamae[1,2], Tomoo Ogura[3], Masahiro Watanabe[4], Shang-Ping Xie[2], and Hiroaki Ueda[1]

[1]Faculty of Life and Environmental Sciences, University of Tsukuba, Tsukuba, Japan, [2]Scripps Institution of Oceanography, University of California, San Diego, La Jolla, California, USA, [3]Center for Global Environmental Research, National Institute for Environmental Studies, Tsukuba, Japan, [4]Atmosphere and Ocean Research Institute, University of Tokyo, Kashiwa, Japan

Abstract Cloud-related radiative perturbations over land in a warming climate are of importance for human health, ecosystem, agriculture, and industry via solar radiation availability and local warming amplification. However, robustness and physical mechanisms responsible for the land cloud feedback were not examined sufficiently because of the limited contribution to uncertainty in global climate sensitivity. Here we show that cloud feedback in general circulation models over tropical land is robust, positive, and is relevant to atmospheric circulation change and thermodynamic constraint associated with water vapor availability. In a warming climate, spatial variations in tropospheric warming associated with climatological circulation pattern result in a general weakening of tropical circulation and a dynamic reduction of land cloud during summer monsoon season. Limited increase in availability of water vapor also reduces the land cloud. The reduction of land cloud depends on global-scale oceanic warming and is not sensitive to regional warming patterns. The robust positive feedback can contribute to the warming amplification and drying over tropical land in the future.

1. Introduction

An enormous uncertainty still remains in the amplitude of global-scale climate response to anthropogenic forcing [*Knutti and Hegerl*, 2008; *Intergovernmental Panel on Climate Change*, 2013]. Intermodel spread in cloud feedback is the largest contributor for the uncertainty in equilibrium climate sensitivity, determined as global mean surface air temperature (SAT) change in response to CO_2 doubling [*Dufresne and Bony*, 2008]. Among different types of clouds (region, height, and optical depth), cloud feedback over the ocean, particularly associated with subtropical low cloud [e.g., *Bony and Dufresne*, 2005; *Brient and Bony*, 2013; *Blossey et al.*, 2013; *Zhang et al.*, 2013; *Demoto et al.*, 2013; *Dal Gesso et al.*, 2015], is an important contributor to the spread of equilibrium climate sensitivity among climate models [*Webb et al.*, 2006; *Vial et al.*, 2013; *Zelinka et al.*, 2013, hereafter Z13; *Qu et al.*, 2015a, 2015b]. *Sherwood et al.* [2014] revealed that efficiency in water vapor transport from the wet boundary layer to dry free troposphere via lower tropospheric mixing can explain a large part of the intermodel spread in low-cloud feedback and resultant uncertainty in equilibrium climate sensitivity.

In addition to the global mean climate response, understanding regional climate changes is one of the grand challenges for climate science [*Xie et al.*, 2015]. For a better understanding of regional properties of climate changes, atmospheric circulation change including the general weakening of tropical circulation [*Held and Soden*, 2006; *Ma et al.*, 2012] and shifts in convergence and subsidence regions [*Xie et al.*, 2010; *Ma et al.*, 2012; *Ma and Xie*, 2013; *Chadwick et al.*, 2013; *Huang et al.*, 2013; *He and Soden*, 2015] holds the key because of the contribution both to zonal mean [*Yin*, 2005; *Lu et al.*, 2007; *Seidel et al.*, 2008; *Grise and Polvani*, 2014] and zonally asymmetric [*Chou and Neelin*, 2004; *Ueda et al.*, 2006; *Vecchi and Soden*, 2007; *Chou et al.*, 2009] climate changes. In addition, contrast in climate response between land and sea also contributes to regional climate change formation [e.g., *Manabe et al.*, 1991]. Through the land-sea contrast, atmospheric circulation response to spatially uniform external forcing exhibits regional patterns [e.g., *Joshi et al.*, 2008; *Li et al.*, 2012; *Bayr and Dommenget*, 2013; *Kamae et al.*, 2014b; *Shaw and Voigt*, 2015]. In addition, the projected changes over land influence directly on human health, economic activity, natural disaster, agriculture, and land ecosystems [e.g., *Dai*, 2013; *Kamae et al.*, 2014a; *Seneviratne et al.*, 2014; *Good et al.*, 2015; *Chadwick et al.*, 2015; *Burke et al.*, 2015].

In the previous literatures, the land cloud feedback has not attracted much attention because of its limited contribution to the uncertainty in global climate sensitivity [e.g., *Vial et al.*, 2013]. In a warming climate, land surface exhibits a larger warming than the ocean and a reduction of relative humidity (RH) because of limited water vapor availability [e.g., *Manabe et al.*, 1991; *Joshi et al.*, 2008; *O'Gorman and Muller*, 2010; *Feng and Fu*, 2013;

Sherwood and Fu, 2014]. With the limited increase in water vapor supply from the ocean, convective systems over land in summer monsoon tend to be suppressed in a warming climate [*Fasullo*, 2012; *Endo and Kitoh*, 2014]. Such thermodynamic constraints due to a limited increase in evapotranspiration and low-level water vapor advection from the ocean were suggested to be important for reductions of cloud and RH in the boundary layer over land in global warming projections [*Fasullo*, 2010]. However, the above studies did not distinguish cloud changes due to different physical processes. The cloud response to external radiative forcing consists of cloud feedback and rapid adjustment. Here the rapid adjustment is independent of the sea surface temperature (SST) change [*Kamae et al*., 2015a; *Sherwood et al*., 2015; Z13] and is distinguished from the slow response mediated by SST change. The two have distinct effects on the regional changes in clouds and atmospheric circulations [*Deser and Phillips*, 2009; *Bony et al*., 2013; *Chadwick et al*., 2014; *Kamae et al*., 2014b, 2015a; *Shaw and Voigt*, 2015]. Quantifying the direct response to imposed external forcing, the indirect effect of increasing SST and its spatial pattern are important for physical understanding of the global and regional climate changes.

In this study, we investigated changes in cloud properties over land and quantified the uncertainty range based on multiple climate model simulations. We examined the associated atmospheric circulation change by quantifying contributions of the direct response, globally uniform oceanic warming, and patterned SST increase. Results of this study suggest that uncertainty in the land cloud feedback is small despite large uncertainties in the spatial pattern of SST increase and relevant regional changes in atmospheric circulation and hydrological cycle in a warming climate [*Shiogama et al*., 2011; *Ma et al*., 2012; *Ma and Xie*, 2013; *Chadwick et al*., 2013; *Huang et al*., 2013; *Endo and Kitoh*, 2014; *Long et al*., 2016]. This is because the land cloud feedback is largely determined by the thermodynamic constraints and physically robust changes in seasonal and regional atmospheric circulations anchored by climatological atmospheric circulation. The rest of the paper is organized as follows. Section 2 describes the data and methods used. Section 3 investigates land cloud change, associated changes in the atmospheric circulation and the thermodynamic structure, and robustness of land cloud feedback. In section 4, we examine physical mechanisms responsible for the cloud change found in atmosphere-only and atmosphere-ocean couple climate model simulations. Section 5 presents relationship between the land cloud feedback and land-sea warming contrast. In section 6, we present a summary and discussion on this study.

2. Data and Methods

2.1. Models and Experiments

We use results of model simulations archived by the Coupled Model Intercomparison Project phase 5 (CMIP5) [*Taylor et al*., 2012]. To examine cloud feedback over tropical land, variables associated with cloud (total cloud amount, hereafter Clt; cloud fraction in model layers, hereafter Cl; and satellite cloud simulator outputs; see section 2.2), dynamic circulation (vertical pressure velocity, hereafter ω), and thermodynamic structure (temperature and RH) were used in this study. All the model outputs are interpolated into $2.8° \times 2.0°$ grid. Using other interpolations (e.g., $2.0° \times 2.0°$) does not change the results substantially. In CMIP5, Cl was provided as values at individual model layers. In this study, Cl was interpolated vertically into 17-layer pressure coordinate (similar to temperature, RH, and ω). Eight models were selected (Table 1) because of limited data availability in CMIP5 (particularly for satellite cloud simulator outputs). To confirm the robustness of cloud changes found in eight models, outputs from additional two models were also examined (Table 1; see section 4.2) although variables associated with satellite cloud simulator were not available for these models.

We use data from the following experiments: amip, amip4K, amipFuture, amip4xCO2, piControl, and 1%CO2 [*Taylor et al*., 2012]. In atmosphere-ocean coupled general circulation models (CGCMs), preindustrial control simulation (piControl) and 1% yr^{-1} CO_2 increase experiment (1%CO2) were performed to examine transient responses to increasing CO_2. In atmosphere-only general circulation models (AGCMs), Atmospheric Model Intercomparison Project (AMIP)-type control simulation (amip) and the three sensitivity experiments were performed. In amip4K and amipFuture, spatially uniform sea surface temperature (SST) increase of 4 K and spatially patterned SST increase were added on the observed SST prescribed in amip. The spatially patterned SST increase was derived from the ensemble mean from transient CO_2 increase experiments conducted in CMIP3 CGCMs [*Taylor et al*., 2012]. Here the spatially patterned SST increase was scaled for a global mean increase in SST of 4 K.

In this study, changes in cloud and associated variables are compared among the different CMIP5 simulations. Here difference of the two AGCM runs (amip4K minus amip) cannot be compared with 1%CO2 directly

Table 1. Change in Total Cloud Amount Over Tropical Land[a]

	USST	CGCM	RCP4.5 (21C)	RCP4.5 (22C)	RCP4.5 (23C)
CNRM-CM5	3.23	-2.27	-0.86	-0.99	-1.35
CanAM4/CanESM2	-4.95	-5.54	-3.94	-4.15	-4.20
HadGEM2-A/HadGEM2-ES	-3.77	-3.07	-2.20	-2.47	-2.41
IPSL-CM5A-LR	-3.16	-3.60	-2.31	-2.44	-2.77
IPSL-CM5B-LR	-3.23	-5.56	-2.01		
MIROC5	-4.43	-4.17	-1.46		
MPI-ESM-LR	-3.99	-4.94	-2.28	-3.14	-3.25
MRI-CGCM3	-3.14	-2.49	-1.13		
MME (eight models)	-3.74 ± 0.63	-3.96 ± 1.22	-2.02 ± 0.88	-2.64 ± 1.19	-2.80 ± 1.09
CCSM4	-3.21	-1.70	-0.80	-0.85	-1.15
MPI-ESM-MR	-3.82	-4.48	-1.87		
MME (all models)	-3.69 ± 0.59	-3.78 ± 1.31	-1.89 ± 0.90	-2.34 ± 1.07	-2.52 ± 0.98

[a]Values represent changes (%) averaged over 20°S–20°N. Upper eight models are used in Figures 1–9. Value in multimodel ensemble (MME) row represents MME mean and its $\pm 1\sigma$. USST column represents 30 year averaged change in amip4K compared with amip. The values were scaled for global mean change in surface air temperature (ΔSATg) of 3.67 K (see section 2.1). CGCM represents anomaly in 1%CO2 run compared with piControl run. RCP4.5 columns are anomalies averaged in years 2070–2099 (21C), 2170–2199 (22C), and 2270–2299 (23C) compared with years 1950–1999 in the historical run.

because (1) the former does not contain the effect of rapid adjustment to increasing CO_2 [*Kamae et al*., 2015a; Z13] and (2) global warming amplitudes (e.g., global mean SAT change, hereafter ΔSATg) are not identical between 1%CO2 and the difference of the AGCM runs (Table S1 in the supporting information). In addition, the cloud feedback diagnosed in the AMIP-type simulations could be biased compared with that in CGCMs because of lack of air-sea interaction. However, *Ringer et al*. [2014] reported that cloud feedback parameters showed good agreement between AMIP-type simulations and CGCMs. Therefore, we compared cloud changes simulated in AGCMs and CGCMs according to decomposition methods used in previous studies [*Kamae et al*., 2014a; *He and Soden*, 2015].

First, anomalies in 1%CO2 and AGCM-based idealized simulations are calculated by comparing with control simulations as below:

$$+4\mathrm{K} = [\mathrm{amip4K}_{1979-2008}] - [\mathrm{amip}_{1979-2008}] \quad (1)$$

$$+\mathrm{Pattern} = [\mathrm{amipFuture}_{1979-2008}] - [\mathrm{amip}_{1979-2008}] \quad (2)$$

$$\mathrm{CO_2} = [\mathrm{amip4xCO2}_{1979-2008}] - [\mathrm{amip}_{1979-2008}] \quad (3)$$

$$\mathrm{CGCM} = [1\%\mathrm{CO2}_{111-140}] - [\mathrm{piControl}] \quad (4)$$

where [ ] and subscripts represent averages for the given periods. Time periods for piControl were set to be identical to 1%CO2 run. Next, ΔSATg was used for determining scaling factors $f1$ and $f2$ to reconstruct changes in CGCM as below:

$$f1 = (\Delta\mathrm{SATg}_{\mathrm{CGCM}} - \Delta\mathrm{SATg}_{\mathrm{CO2}})/\Delta\mathrm{SATg}_{+4\mathrm{K}} \quad (5)$$

$$f2 = (\Delta\mathrm{SATg}_{\mathrm{CGCM}} - \Delta\mathrm{SATg}_{\mathrm{CO2}})/\Delta\mathrm{SATg}_{+\mathrm{Pattern}} \quad (6)$$

$$\mathrm{USST} = +4\ \mathrm{K}f1 \quad (7)$$

$$\mathrm{PAT} = +\mathrm{Pattern}f2 \quad (8)$$

$$\mathrm{Sum} = \mathrm{PAT} + \mathrm{CO_2} \quad (9)$$

$$\mathrm{Residual} = \mathrm{CGCM} - \mathrm{Sum} \quad (10)$$

Here eight-model mean ΔSATg in +4K, +Pattern, CO_2, and CGCM equal to 4.61, 4.86, 0.50, and 3.67 K, respectively (Table S1). Resultant $f1$ and $f2$ are 0.80 and 0.76 in eight-model mean. $f1$ in the individual models are listed in Table S1. In this study, anomalies in response to the spatially uniform ΔSST in given variables like Clt (ΔClt) are shown as USST. Resultant Δ represents a change per 3.67 K increase in global mean SAT, corresponding to $\Delta\mathrm{SATg}_{\mathrm{CGCM}}$ minus $\Delta\mathrm{SATg}_{\mathrm{CO2}}$.

In section 4.2, we also used the results of the historical run and future climate projection under the Representative Concentration Pathway (RCP) 4.5 conducted in CGCMs [*Meinshausen et al*., 2011; *Taylor et al*., 2012]. Here CGCMs are coupled models using the above AGCMs as the atmospheric component. All

the 10 models provided outputs for historical (1860–2005) and RCP4.5 run before 2100. Six models were used for analyses after 2101 because of data availability (Table 1).

2.2. ISCCP Simulator and Cloud Radiative Kernel

To diagnose cloud feedbacks in CMIP5 models, we use the method of Z13. First, the satellite cloud simulator implemented in the CMIP5 models translated Cl in the individual model layers into a distribution of cloud fraction as a joint function of cloud top pressure (CTP) ranges and cloud optical depth (τ) ranges in a similar manner to the satellite observation. In this study, we used the International Satellite Cloud Climatology Project (ISCCP) simulator [*Klein and Jakob*, 1999; *Webb et al*., 2001] that diagnose 49 types of cloud (seven CTP and seven τ bins). We conclude that the cloud simulators were implemented properly in all the eight models because the sum of all the diagnosed cloud fractions matches well with the model-produced Clt (figure not shown; Z13).

Next, the simulator-produced 49 types of clouds were used to diagnose cloud feedback. M. Zelinka kindly provided ISCCP cloud radiative kernel (Z13) calculating cloud feedback based on the ISCCP cloud fractions and surface albedo. By using this cloud radiative kernel, we can diagnose radiative perturbation at the top-of-the-atmosphere (TOA) due to change in simulated clouds in the models. The sum of TOA radiation from all the 49 types of clouds represents total cloud feedback. Then a partitioning method proposed in *Zelinka et al*. [2012b] and Z13 was applied to decompose the total cloud feedback into (1) cloud amount feedback, (2) CTP feedback, (3) τ feedback, and (4) residual. The cloud amount feedback was calculated by assuming constant relative proportions of cloud fractions in each CTP-τ bin between control and perturbed climates. Resultant proportionate change in the cloud fraction corresponds to the cloud amount feedback [*Zelinka et al*., 2012b]. Z13 reported that global mean cloud amount feedback among five models are robustly positive and negative in shortwave (SW) and longwave (LW) components, respectively. A larger feedback of the former (SW) than the latter (LW) results in a robust positive net (sum of SW and LW) cloud amount feedback. This is because TOA radiative perturbation due to changes in cloud fraction is larger in SW than LW except high-level cloud [*Kiehl and Ramanathan*, 1990]. Note that CTP and τ feedback also contribute to the total cloud feedback and its spread among different models (Z13). For example, LW CTP feedback is one of the largest contributors to the uncertainty in the total cloud feedback (Figure 3 in Z13).

One of the merit using the ISCCP cloud radiative kernel to diagnose cloud feedback is that the diagnosed feedback parameter is independent from "cloud masking" problem [*Soden et al*., 2008]. From direct model outputs, cloud radiative effect can be calculated by comparing all-sky and clear-sky TOA radiation. However, the cloud radiative effect estimated by this method contains radiative perturbation due to noncloud processes [*Soden et al*., 2008; Z13]. Influences of the cloud masking effect are substantial for both global and regional cloud feedback estimates. In this study, we calculated cloud feedback by using ISCCP cloud radiative kernel because it is an effective method to diagnose the feedback parameter without contaminations of the noncloud effect. Although several limitations in the method of ISCCP cloud radiative kernel (e.g., finite resolution of CTP-τ bins and obscuration effects) were suggested in *Zelinka et al*. [2012a] and Z13, we applied this method to compare cloud feedback among different models from available multimodel data archive. We confirmed that using a SW cloud radiative effect does not change the results of this study substantially (figure not shown). In addition, derived cloud feedback is generally consistent with ΔClt computed directly in individual models (see section 3.2).

3. Cloud Change in Response to Ocean Warming

3.1. Total Amount and Vertical Structure of Cloud

In this section, we examine changes in Clt and associated variables in response to the spatially uniform ΔSST simulated in the eight models. Here ΔClt in response to the spatially uniform ΔSST resembles to that simulated in CGCMs (see section 4.2). Figure 1 shows spatial patterns of changes in Clt, ω at 500 hPa level (ω_{500} hereafter), boundary layer RH, and precipitation. Here Δ shown in Figure 1 is +4K anomaly, scaled for ΔSATg of 3.67 K (USST; see section 2.1). More details of the spatial patterns of ω_{500} and precipitation can be found in Figure 2. Spatial patterns of USST are compared with Sum and CGCM in section 4.2. ΔClt is generally negative over the middle latitude (Figure 1a) associated with the poleward expansion of the Hadley cells [*Lu et al*., 2007; *Seidel et al*., 2008]. Over the low latitude, substantial Clt reduction can also be found,

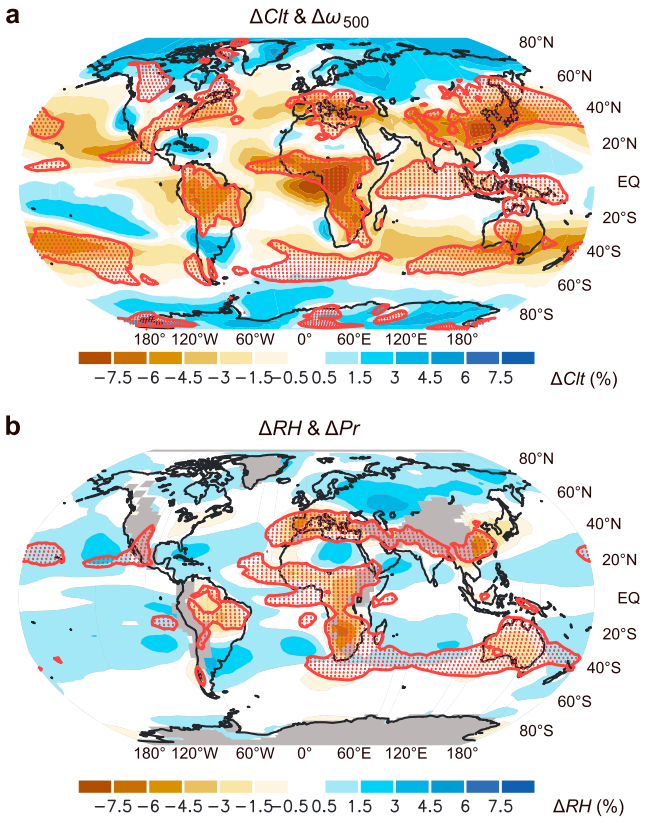

Figure 1. (a) Annual mean, eight-model mean changes in total cloud amount (ΔClt hereafter; shading; %) and ω at 500 hPa level ($\Delta\omega_{500}$ hereafter; dotted area with red contour represent $\Delta\omega_{500} > 2$ hPa d^{-1}) in response to spatially uniform SST increase (USST). The shown anomalies are scalded for a global mean ΔSAT of 3.67 K (in eight-model mean; see section 2.1). (b) Change in relative humidity (ΔRH) averaged from 850 to 1000 hPa levels (shading; %). Dotted area with red contour represents precipitation change less than -0.05 mm d^{-1}.

but it is largely confined to land regions, distinct from the more zonally uniform reduction of Clt over the middle latitude. This suggests a different physical mechanism for the midlatitude cloud reduction. ΔClt listed in Table 1 indicates that the reduction of Clt over tropical land is robust among eight models.

Previous studies suggested that changes in atmospheric circulation and thermodynamic structure (temperature and RH) are the keys to change in Clt (particularly in middle and high cloud fractions) in a perturbed climate [e.g., *Bony et al.*, 2004, hereafter B04; *Watanabe et al.*, 2012; *Kamae and Watanabe*, 2012, 2013]. Here the large-scale atmospheric circulation shows a positive downward anomaly ($\Delta\omega_{500} > 0$) over tropical land (Figures 1a and 2). The strong cloud reduction over tropical South America, tropical Africa, and weak cloud changes over the Sahara, Arabian Peninsula, and South Asia correspond well with the spatial pattern of $\Delta\omega_{500}$ (Figures 1a and 2), suggesting the importance of the change in atmospheric circulation for the negative ΔClt over tropical land.

Figure 1b shows change in total precipitation and lower tropospheric RH. Spatial patterns of changes in Clt and precipitation over tropical land are similar to that in RH. The boundary layer becomes dryer over tropical land in a warming climate due to the limited moisture availability [e.g., *O'Gorman and Muller*, 2010; *Feng and Fu*, 2013]. In a globally warming world, while global mean precipitation increases [*Allen and Ingram*, 2002; *Held and Soden*, 2006], the precipitation change shows substantial regionality (including both positive and negative signs) associated with changes in the large-scale atmospheric circulation (Figures 1 and 2) [*Chadwick et al.*, 2013; *Endo and Kitoh*, 2014; *Xie et al.*, 2015]. Details of the precipitation change associated with atmospheric circulation in +4K were examined in previous studies [*Ma and Xie*, 2013; *Huang*, 2014; *He et al.*, 2014]. Here negative ΔClt and ΔRH are found not only over the continents but also over the Malay Archipelago.

Figure 3 shows changes in Cl and Clt over land. Vertical profiles of tropical mean (20°S–20°N) ΔCl and ΔRH are shown in Figure 4. ΔCl in individual model layers (Figures 3a and 4a) shows the following: (1) a reduction from the lower to upper troposphere, (2) an upward shift of cloud layer in the upper troposphere (gray and red lines in Figure 4a), and (3) a strong reduction in the middle latitudes (Figures 3a and 3b) associated with the poleward expansion of the Hadley circulation [e.g., *Mitchell and Ingram*, 1992; *Lu et al.*, 2007]. Vertical profile of ΔRH (general drying; Figure 4b) is similar to that in ΔCl except upper troposphere (Figure 4a). Negative ΔClt over tropical land is large and robust among the models (Figure 3b and Table 1) although zonal mean change including the ocean is not robust [*Zelinka et al.*, 2012a; Z13]. Figures 3c, 3d, and 4c show land-sea contrasts in ΔCl and ΔClt. The cloud reduction over tropical land is larger than that over the ocean from the lower to upper troposphere (Figures 3c and 4c), resulting in a land-sea contrast in ΔClt over the tropics (Figure 3d). The tropospheric drying (negative ΔRH) is always larger over land than the ocean from the surface to 300 hPa (Figure 4d), corresponding to the ΔCl contrast (Figures 3c and 4c). Note that clear land-sea ΔClt contrast cannot be found around 20°N (Figure 3d) due to high cloud reduction (Figure 3c) over the Sahara, Arabian Peninsula, and South Asia (Figure 1a).

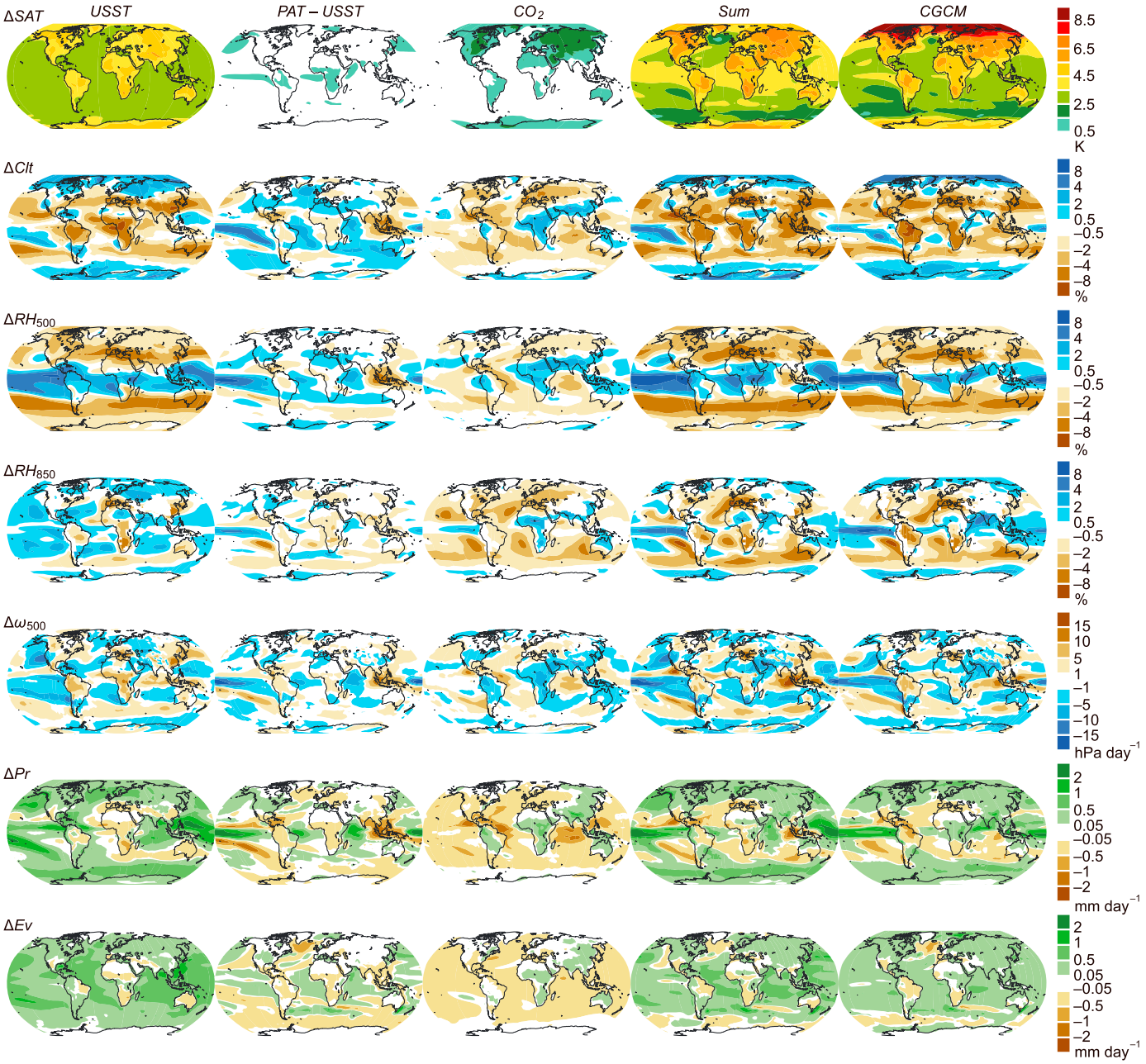

Figure 2. Maps for USST, PAT, CO_2, Sum, and CGCM simulated in eight AGCMs/CGCMs (Table 1). Definitions of these components can be found in section 2.1. (from top to bottom) Anomalies of surface air temperature (ΔSAT; K), ΔClt (%), ΔRH at 500 hPa level (%) and 850 hPa level, ω at 500 hPa level ($\Delta\omega_{500}$; hPa d^{-1}), precipitation (mm d^{-1}), and evaporation (mm d^{-1}).

Previous studies suggested a RH reduction in the boundary layer over land in a warming climate because neither surface evapotranspiration nor horizontal moisture advection from ocean can increase enough to maintain a constant RH [e.g., *O'Gorman and Muller*, 2010; *Fasullo*, 2010; *Sherwood and Fu*, 2014]. The above results support the moisture constraints in USST. However, the largest Cl reduction is found in the middle to upper troposphere (Figures 3 and 4). In addition, the regionality of ΔClt corresponds well with the change in large-scale atmospheric circulation (Figures 1a and 2), suggesting the importance of the dynamic cloud change. In section 4.1, factors contributing to the change in the tropical atmospheric circulation and land cloud are examined.

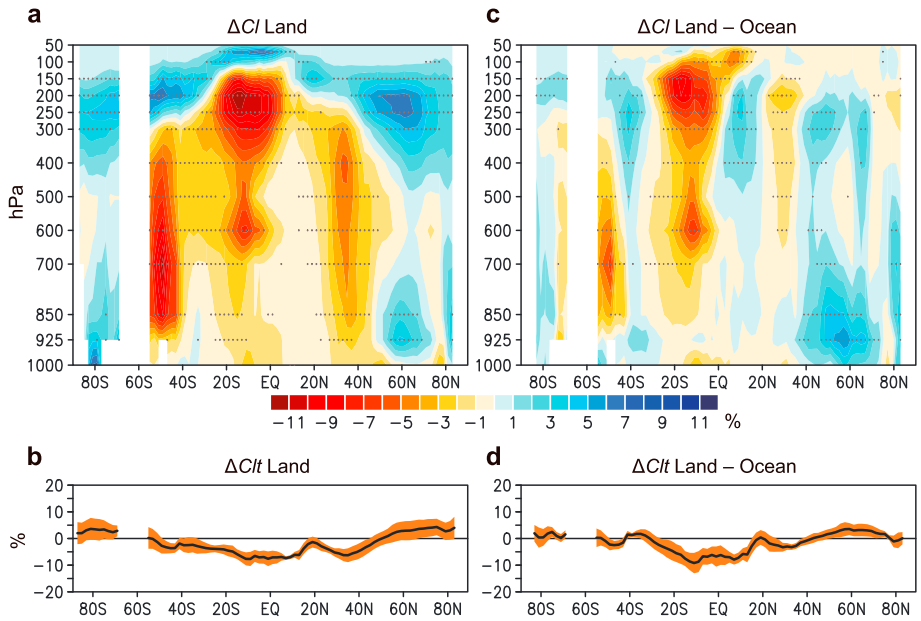

Figure 3. (a) Zonal mean change in cloud fraction (ΔCl; %) over land in USST averaged among eight models. Cl is interpolated into 17 levels of pressure coordinate. Stipples denote regions where the absolute values of anomalies are larger than 1σ. (b) Zonal mean ΔClt (%) over land. Shading represents ±1σ. (c, d) Similar to Figures 3a and 3b but for land minus ocean.

3.2. Shortwave Cloud Feedback

The negative ΔClt over tropical land found in USST could result in a positive SW cloud feedback. Figure 5 shows spatial patterns of SW cloud feedback parameter determined as TOA radiative perturbation due to cloud change per ΔSATg and its cloud amount feedback component (section 2.2) averaged among eight models. We can confirm that the spatial pattern over the tropics (Figure 5a) is quite similar to that in ΔClt (with reversed sign; Figure 1a) and SW cloud amount feedback (Figure 5b), suggesting a dominant contribution of cloud amount feedback. In contrast, SW cloud amount feedback (Figures 5b, 5d, and 5f) is not sufficient to explain large negative SW cloud feedback found over the high latitude (Figures 5a, 5c, and 5e). As noted in previous studies [*Vial et al.*, 2013; Z13], the SW cloud feedback is robustly negative over the high latitude associated with increasing τ [*Zelinka et al.*, 2012b; *Ceppi et al.*, 2016; Z13]. Over the middle latitude, SW cloud feedback and its cloud amount feedback component are robustly positive associated with the reduction of Clt (Figures 1a and 5a–5f). SW cloud feedback over

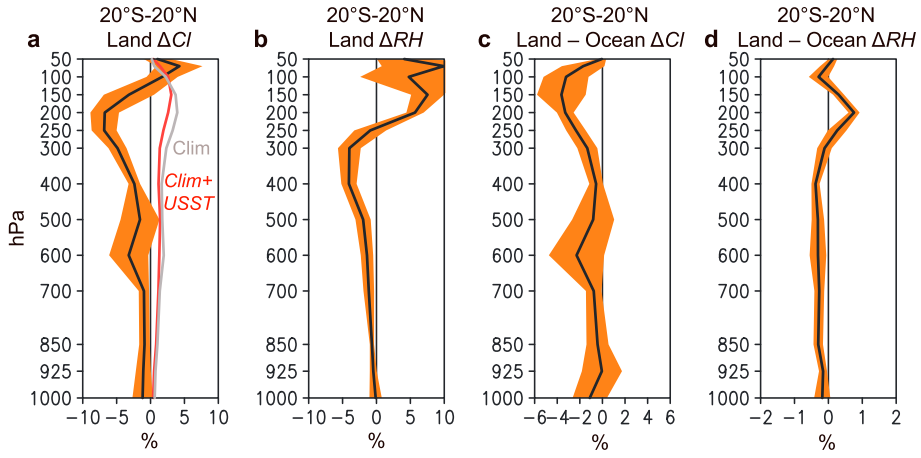

Figure 4. (a) Similar to Figure 3a but for 20°S–20°N mean (black line). Shading represents ±1σ. Gray and red lines are climatology in amip and USST plus the amip climatology, respectively. Both of the two are divided by 5. (b) Similar to Figure 4a but for ΔRH (%). (c, d) Similar to Figures 4a and 4b but for land minus ocean.

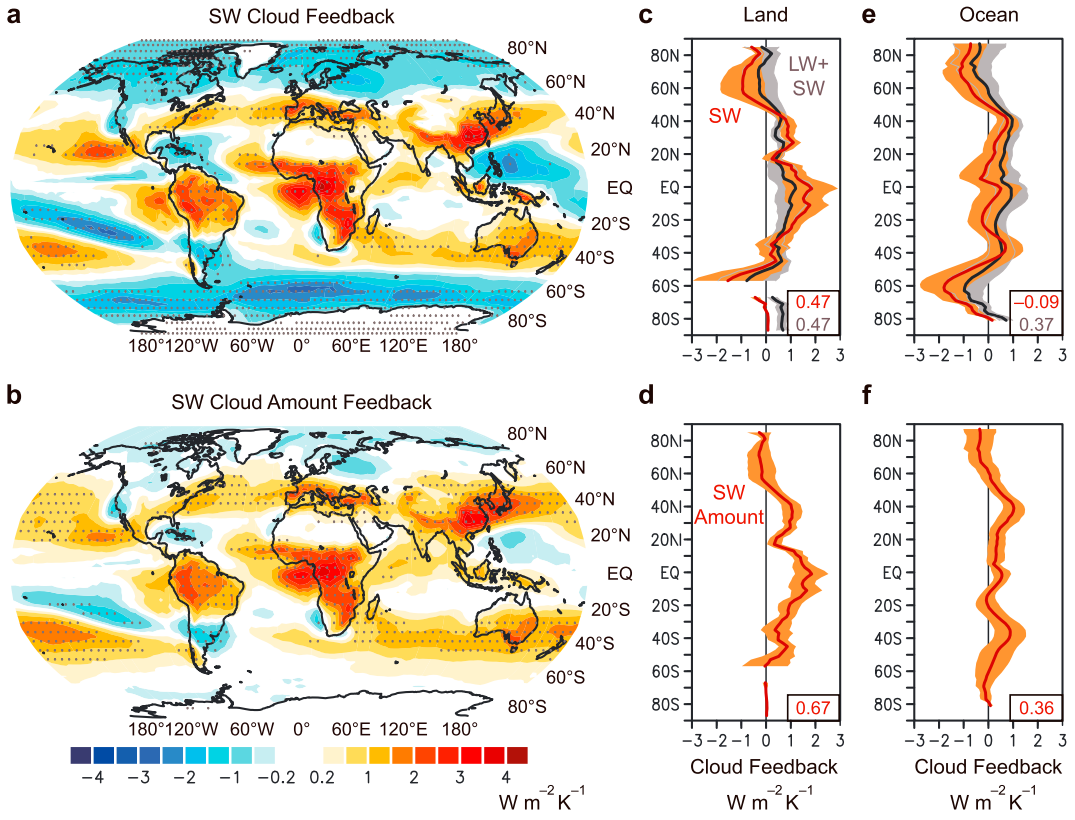

Figure 5. Cloud feedback parameter (W m^{-2} K^{-1}) diagnosed using ISCCP simulator and cloud radiative kernel in amip4K run. (a) Shortwave (SW) cloud feedback and (b) SW cloud amount feedback. Stipples denote regions where the absolute values of anomalies are larger than 1σ. (c) Zonally averaged cloud feedback parameter over land and (e) ocean. Orange and black lines indicate SW and net (SW plus longwave) cloud feedback, respectively. Shadings represent ±1σ. Values shown in lower right represent global means (orange is SW; gray is net). (d, f) Similar to Figures 5c and 5e but for SW cloud amount feedback.

tropical land is robustly positive (except over North Africa, Arabian Peninsula, and South Asia) and larger than the ocean (Figures 5a and 5e), consistent with the larger reduction of Clt (Figures 1a, 3b, 3d, 5d, and 5f). It is interesting that the positive SW cloud feedback over land was also found systematically in a superparameterized global climate model that explicitly simulates cumulus convections [*Bretherton et al.*, 2014]. The consistency among the different model simulations suggests a robust physical mechanism responsible for the cloud feedback (see section 4.1). Compared with the other components (CTP feedback, τ feedback, and residual; not shown), the cloud amount feedback (1.3 W m^{-2} K^{-1}) dominates the total cloud feedback over tropical land.

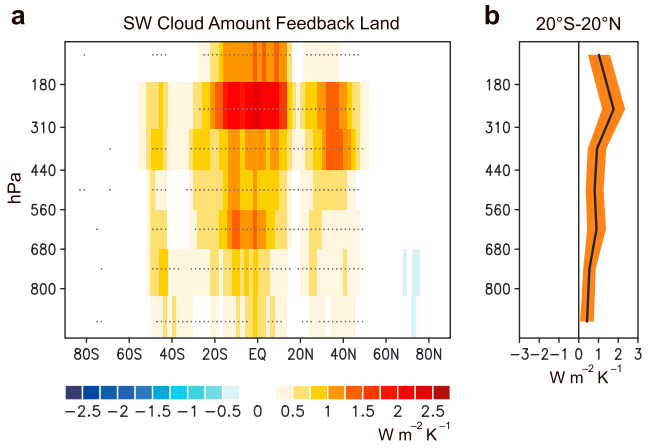

Figure 6. (a) Latitudinal and cloud top height distribution of SW cloud amount feedback (W m^{-2} K^{-1}) over land in amip4K run. Stipples indicate regions where the absolute values of anomalies are larger than 1σ. (b) 20°S–20°N mean. Shading represents ±1σ.

LW cloud feedback (black minus orange in Figures 5c and 5e) is robustly positive over the high-latitude land and generally negative (positive) over the low-latitude land (ocean), as shown in Z13. Although the positive SW cloud feedback over tropical land (1.3 W m^{-2} K^{-1} in eight-model mean)

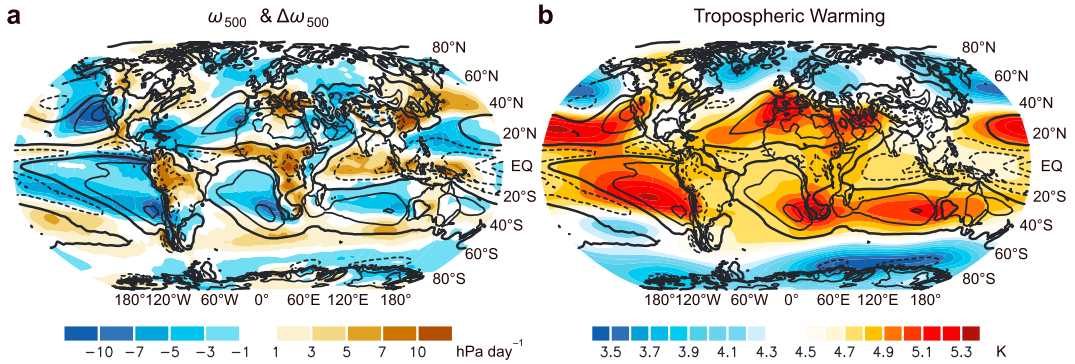

Figure 7. Relationship between atmospheric circulation in amip run and its change in USST. (a) Eight-model mean of $\Delta\omega_{500}$ (shading; hPa d^{-1}) and ω_{500} (contour; ±20, 10, and 0 hPa d^{-1}). Dashed and solid contours represent negative and positive ω_{500}. Thick contour represents 0 hPa d^{-1}. (b) Similar to Figure 7a but for tropospheric warming (shading; K) averaged from 300 to 850 hPa levels. Contours are identical to Figure 7a.

is partly offset by LW component, net cloud feedback (0.8 W m^{-2} K^{-1}) is also robustly positive among eight models (Figure 5c). This cloud feedback can contribute to local amplification of land surface warming in USST (Figure 2). However, the positive cloud feedback also shows a substantial intermodel spread (Figures 5c and 5d), suggesting a possible contribution to intermodel spread in land surface warming (see section 5).

Figure 6 shows the vertical distribution of zonal mean SW ISCCP cloud amount feedback over land. The cloud fraction diagnosed with the ISCCP cloud simulator in individual models tends to decrease in the warming condition, resulting in a positive SW cloud amount feedback. Here the large positive SW cloud amount feedback is confined to the middle and low latitudes (Figure 6a) with peaks in middle to high CTPs over the Northern Hemisphere and Southern Hemisphere middle latitudes and tropics (Figure 6b). Although the CTP of ISCCP low-level cloud could be biased partly [e.g., *Garay et al.*, 2008], the direct output of Cl (Figures 3a and 4a) also supports that the positive SW cloud amount feedback can be found in the deep troposphere.

4. Physical Mechanisms

4.1. Dynamic and Thermodynamic Cloud Changes

As shown in previous sections, the spatial patterns of changes in atmospheric circulation and thermodynamic structures correspond well with the cloud reduction over tropical land. In this section, we examined physical mechanisms responsible for the robust cloud change over tropical land. Figure 7a shows a global map of ω_{500} in amip, and its change in USST. The spatial pattern in $\Delta\omega_{500}$ is similar to climatological ω_{500} (negative correlation, $R = -0.49$ over 30°S–30°N). The relationship between the two in USST and future projections can be explained by the regional pattern of tropospheric stratification [*Ma et al.*, 2012]. Figure 7b shows the spatial distribution of middle tropospheric warming (300–850 hPa) in USST. Although the imposed ΔSST is spatially uniform, the tropospheric warming shows substantial regionality (e.g., larger warming off the west coast of the continents than in the Intertropical Convergence Zone, hereafter ITCZ). In a warming climate, the upper tropospheric warming is larger than lower and middle troposphere over the tropics [*Manabe and Wetherald*, 1975; *Kamae et al.*, 2015b]. Over climatological subsidence regions, vertical advection by climatological downward flow ($\omega_{500} > 0$) acts as a warm advection, while the climatological ascending motion in the ITCZ ($\omega_{500} < 0$) acts as a cold advection (the first term in the left-hand side of equation 3 in *Ma et al.*, 2012) because of the larger warming in the upper troposphere [*Ma et al.*, 2012, Figure 2]. This Mean Advection of Stratification Change (MASC) [*Ma et al.*, 2012] mechanism induces spatially asymmetric stratification change anchored by the climatological ω, resulting in a general weakening of ω in response to the spatially uniform ΔSST (Figure 7a). The spatial similarity between ω and ΔClt (Figures 1a, 2, and 7) suggests a contribution of the MASC mechanism to the land cloud reduction (detailed below). Note that the MASC-related general weakening of tropical circulation cannot solely explain all the $\Delta\omega_{500}$ patterns in USST because other mechanisms including "upped ante" [*Neelin et al.*, 2003; *Chou et al.*, 2009; *He and Soden*, 2015] also contribute to $\Delta\omega_{500}$.

Interestingly, the spatial ω_{500}-$\Delta\omega_{500}$ correspondence is stronger over land ($R = -0.66$ over 30°S–30°N) than the ocean ($R = -0.44$). The positive $\Delta\omega_{500}$ over tropical land as part of the general weakening of atmospheric

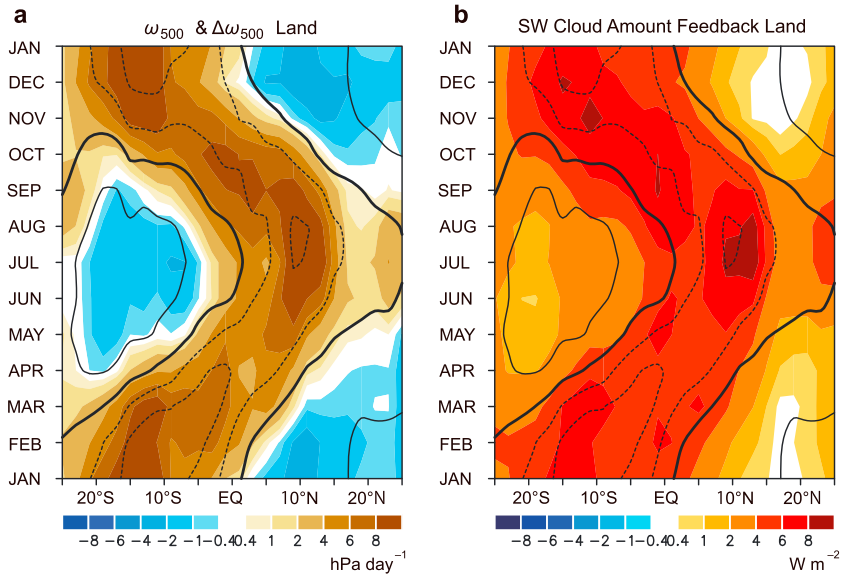

Figure 8. Seasonal variations averaged over land. (a) ω_{500} (contour; ±20, 10, and 0 hPa d^{-1}) and $\Delta\omega_{500}$ (shading; hPa d^{-1}). (b) Similar to Figure 8a but for SW cloud amount feedback in amip4K run (W m^{-2} K^{-1}) times 3.67 K. Contours are identical to Figure 8a.

circulation is consistent among different models because climate models have quite similar spatial patterns of ω_{500} in the control climate. Here the climatological ω over land shows a strong seasonality associated with the seasonal migration of the ITCZ and monsoon. Figure 8 shows seasonal $\Delta\omega_{500}$ and SW cloud amount feedback over tropical land. $\Delta\omega_{500}$ (shading) exhibits a clear seasonality corresponding to the climatological ω (contour). In the Northern (Southern) Hemisphere, strong convective activity from June to August (December to February) weakens in a warming climate and so does subsidence from December to February (June to August). This result suggests that the MASC mechanism can also be applied in the seasonal variation in ω over land, resulting in a larger negative ΔClt and associated increase in SW cloud amount feedback (Figure 8b) during the summer than winter. Here we note that the differential reduction of Clt between land and ocean cannot be explained by the MASC effect (detailed below). In addition, the SW cloud amount feedback is also positive during winter despite negative $\Delta\omega_{500}$ (anomalous ascending motion), suggesting that the dynamic cloud feedback cannot explain the dry-season cloud feedback and other mechanisms are needed. This is consistent with the role of the thermodynamic effect (see section 1) on ΔClt [*O'Gorman and Muller*, 2010; *Fasullo*, 2010; *Sherwood and Fu*, 2014].

Next we compare the relative contributions of the dynamic and thermodynamic cloud changes. Figure 9a shows the histogram of ω_{500} over tropical land in amip and its change in USST. In contrast to the histogram over the ocean (B04), the land histogram (blue bars in Figure 9a) is skewed to the convective regime and maximum in probability is found in a weak subsidence regime (10–20 hPa d^{-1}). The change in ω_{500} histogram (orange bars) exhibits the general weakening of atmospheric circulation (increasing frequency in weak circulation regimes and decreasing in strong circulation regimes). Figure 9b shows Clt in amip run sorted into the circulation regime. Clt exhibits clear circulation regime dependency: more Clt in stronger convective regimes and less Clt in subsidence regimes. In a given perturbed climate, change in probability of ω_{500} can result in a change in Clt because of the circulation regime dependency. For example, increased (decreased) frequencies in weak (strong) convective regime in response to the spatially uniform ΔSST (orange bars in Figure 9a) cause a reduction of Clt. This $\Delta\omega_{500}$-associated ΔClt is referred to as "dynamic cloud feedback" (B04). On the other hand, Clt can change even without any change in the probability distribution of ω_{500}. In USST, Clt is reduced in most of the circulation regimes (Figure 9c). This is called as "thermodynamic cloud feedback." We applied the B04 method for ΔClt over tropical land, then ΔClt can be decomposed as follows:

$$\Delta\mathrm{Clt} = \int \mathrm{Clt}_\omega \Delta P_\omega \mathrm{d}\omega + \int P_\omega \Delta\mathrm{Clt}_\omega \mathrm{d}\omega + \text{residual} \quad (11)$$

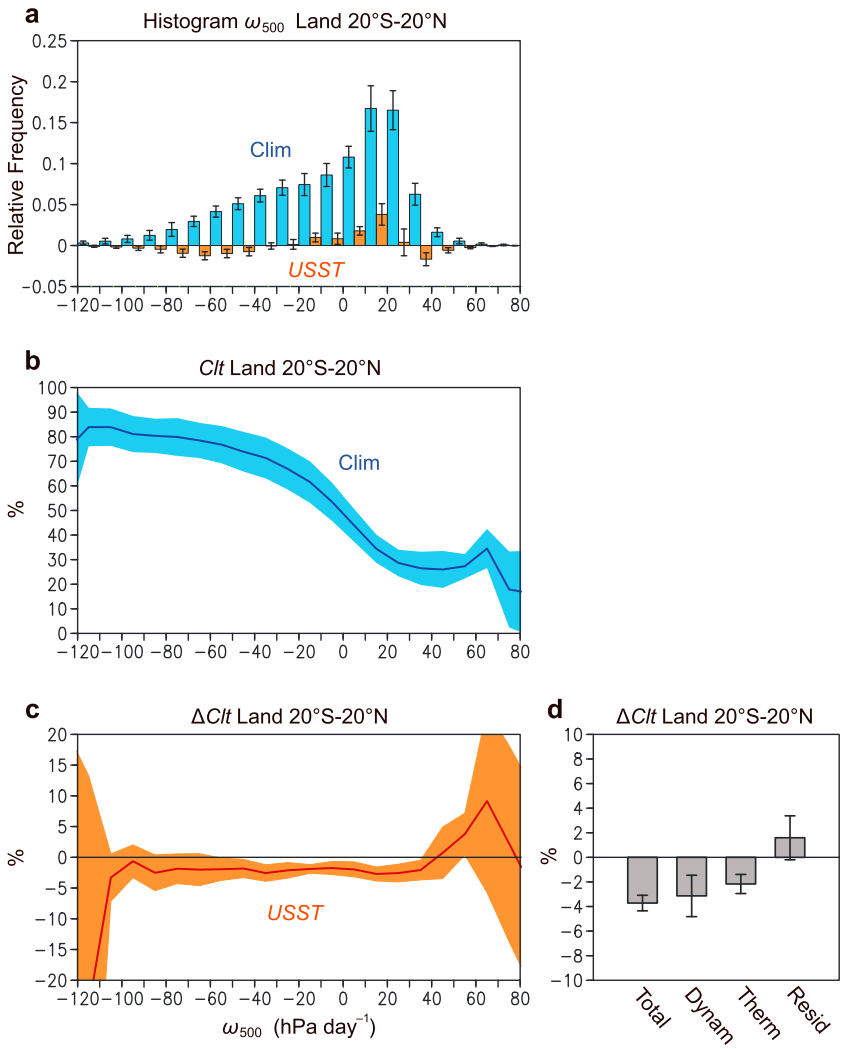

Figure 9. (a) Histogram of ω_{500} (hPa d^{-1}) over tropical land (20°S–20°N) in amip run (blue) and its change in USST (orange). Error bars indicate $\pm 1\sigma$. (b) Clt (%) averaged over the individual bins of ω_{500}. Shading represents $\pm 1\sigma$. (c) Similar to Figure 9b but for ΔClt (%) in USST. (d) ΔClt (%) over tropical land in USST and its decomposition into dynamic, thermodynamic, and residual terms (bars) with their $\pm 1\sigma$ ranges (error bars).

In equation (11), P_ω represents the probability density function of ω_{500}, and Clt_ω is a composite of Clt with respect to ω_{500}. The first and second terms are the dynamic and thermodynamic components. The third term is the residual (covariation) term.

Figure 9d shows the relative contributions of the dynamic, thermodynamic, and residual terms to the total ΔClt. Much of the cloud reduction over tropical land can be explained by the dynamic component. In general, the thermodynamic component dominates the oceanic cloud feedback (B04). In contrast, the robust change in the seasonal and regional ω over tropical land (Figure 8a) results in the substantial dynamic term. Here we should note that the residual term and intermodel spread in the dynamic term are not negligible. Large changes both in P_ω and thermodynamic cloud amount result in the substantial covariation term over tropical land. We conclude that the dynamic contribution is largely comparable to the thermodynamic term, but the relative importance is model dependent (error bars in Figure 9d).

As shown above, the apparent land-sea ΔClt contrast can be found over the tropics (Figure 3d). However, the MASC mechanism cannot solely explain the land-sea ΔClt contrast. The climatological negative ω_{500} is comparable over the tropical South America, tropical Africa, and the tropical Indian Ocean and western Pacific (contour in Figure 7a). However, the negative ΔClt are clearly larger over tropical land than the ocean

(Figures 1a, 2, and 3d). Here the contribution of the thermodynamic constraints [*O'Gorman and Muller*, 2010; *Fasullo*, 2010; *Sherwood and Fu*, 2014] is important for the larger reduction of ΔClt over land compared with the ocean (Figure 9). These differential ω_{500}-ΔClt relationships between land and ocean should be examined further in future studies.

4.2. Cloud Changes in Patterned SST Increase Runs and Atmosphere-Ocean Coupled Runs

In the previous sections, we showed the importance of the dynamic (Figures 7–9) and thermodynamic (Figures 4 and 9) changes in cloud amount over tropical land in response to the spatially uniform ΔSST. However, in a coupled atmosphere-ocean climate system, anthropogenic radiative forcing induces a spatial asymmetry in ΔSST [*Mizuta et al*., 2014] through air-sea interactions [*Xie et al*., 2010] and ocean heat uptake [*Flato and Boer*, 2001]. The spatial pattern of multimodel ensemble mean ΔSST and the intermodel variation [*Mizuta et al*., 2014; *Anderson et al*., 2015] may also be important for ΔClt over tropical land. Now we compare ΔClt in USST, PAT, and CGCM (see section 2.1). Here two models (CCSM4 and MPI-ESM-MR) are added to the analyses below (Table 1) to confirm the robustness of the simulated changes.

Changes in Clt and the other variables in Sum shown in Figure 2 are generally similar to CGCM, suggesting linear additivities of these variables. However, there are noticeable differences between the two (i.e., large Residual terms). For example, the polar regions exhibit different warming rates between them. Clt reduction is slightly larger in Sum compared with CGCM (detailed below). These differences may be rooted from the following: (1) the prescribed SST and sea ice are not identical to those simulated in CMIP5 CGCMs and (2) linear additivity does not hold because of nonlinear climate responses [e.g., *Good et al*., 2015; *Knutti and Rugenstein*, 2015]. However, the changes in USST dominate the global changes in CGCM. This result is consistent with previous studies suggesting essential roles of the spatially uniform ΔSST for the tropical circulation changes and poleward expansion of subtropical dry areas [e.g., *Ma et al*., 2012; *Allen et al*., 2014].

ΔSST in CGCM peaks over the equatorial eastern Pacific, equatorial Atlantic, and Northern Pacific [e.g., *Mizuta et al*., 2014]. This ΔSST pattern results in changes in large-scale atmospheric circulation [*Vecchi and Soden*, 2007] in addition to the weakened tropical atmospheric circulation in USST [*Ma et al*., 2012] (see section 4.1). The spatial asymmetry in ΔSST induces a weakening of deep convection over the Maritime Continent and anomalous ascending motion over the eastern equatorial Pacific ($\Delta\omega_{500}$ line, PAT-USST column in Figure 2), resulting in a large reduction and an increase in Clt over the Maritime Continent and the equatorial eastern Pacific, respectively. In addition, the spatial asymmetry in ΔSST decreases Clt over tropical land (ΔClt line in Figure 2), but this effect is small compared with ΔClt induced by the spatially uniform ΔSST. Figure 10 compares ΔClt over tropical land. The spatial asymmetry in ΔSST and CO_2-induced cloud change (without any change in SST) are smaller than USST. This result is consistent with *He et al*. [2014] that changes in precipitation and ω_{500} over tropical land were similar between USST and PAT. Here the direct response to CO_2 increase is referred to as "adjustment" or "rapid response" (see supporting information). Figure 10b shows the relationship between ΔClt over tropical land in USST and CGCM. These two have similar amplitudes and are correlated significantly ($R = 0.59$), suggesting that ΔClt induced by the spatially uniform ΔSST can largely explain the ensemble mean ΔClt and 38% of the uncertainty found in CGCM.

The above results indicate that the change in the tropical cloud over land can largely be understood by a cloud reduction in USST through the weakening of ω_{500} and the thermodynamic constraints. These results further suggest that the uncertainty in ΔClt is also small in the transient experiments (1%CO2 and realistic RCP4.5) [*Taylor et al*., 2012] despite the substantial uncertainty in ΔSST patterns among models [*Mizuta et al*., 2014; *Long et al*., 2016]. If ΔClt over tropical land is primarily determined by USST, ΔClt should follow global mean ΔSST (and ΔSATg) in RCP simulations. Figure 11 shows the time series of ΔSATg and ΔClt over tropical land simulated in historical and RCP4.5 runs compared with the 1950–1999 mean. In the RCP4.5 run, radiative forcing is nearly constant after 2080 [*Meinshausen et al*., 2011] but ΔSATg continued to increase due to an effect of deep ocean heat uptake [e.g., *Gregory and Mitchell*, 1997]. From the 19th century, Clt over tropical land shows a decreasing trend that accelerates during the 21st century. After 2080, the Clt trend is rather flat but negative during the 22nd and 23rd centuries. The time series of Clt are similar to ΔSATg with reversed sign in all the models. Despite the large intermodel variation in Clt reduction (Table 1 and Figures 3b and 10a), ensemble mean ΔClt and its uncertainty range clearly show decreasing trends after the 21st century. Note that part of the large intermodel spread is attributed to intermodel spread in ΔSATg in the CGCM simulations. Here we did not compare the modeled Clt variation with observations. Currently, substantial

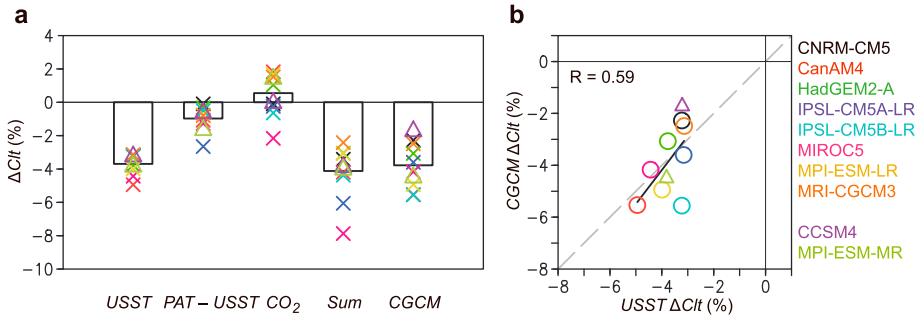

Figure 10. (a) Comparison of ΔClt (%) over tropical land in USST, PAT minus USST, CO_2, Sum, and CGCM (see section 2.1). Purple and green triangles represent the additional two models. (b) A scatter plot of USST and CGCM. Black line represents a least squares regression among 10 models ($R = 0.59$). A dashed line is one-by-one line.

ambiguity remains in the observed global-scale trend in Clt [*Hartmann et al.*, 2013], resulting in a difficulty in evaluating the modeled Clt trend.

5. Land Cloud Feedback and Land-Sea Warming Contrast

As shown above, the intermodel variation in the cloud reduction and associated radiative perturbation (Table 1 and Figures 3b, 5d, and 10a) may influence surface warming amplitude over land. In global warming projections and SST increase experiments, land surface shows a larger warming than the ocean (Figure 2). The land to ocean warming ratio is consistently larger than unity [*Manabe et al.*, 1991; *Sutton et al.*, 2007; *Joshi et al.*, 2008] with substantial intermodel variation (1.3–1.8). Limited heat content, dryer boundary layer and larger lapse rate, limited increase in evapotranspiration, and cloud feedback were suggested to contribute to the land-sea warming contrast [*Manabe et al.*, 1991; *Sutton et al.*, 2007; *Joshi et al.*, 2008; *Kamae et al.*, 2014b]. Recently, *Sejas et al.* [2014] showed that the SW cloud feedback contributes to the land-sea warming contrast by using a climate model simulation and a diagnostic technique. Quantifying sources of intermodel

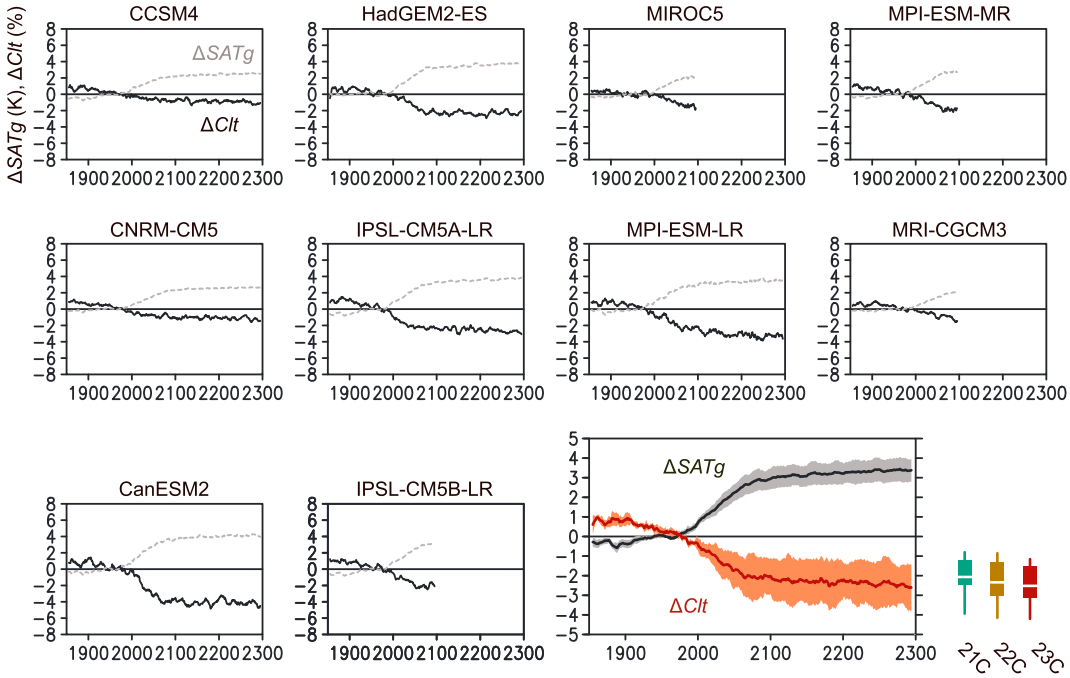

Figure 11. Anomalies of global mean SAT (K) and Clt over tropical land (20°S–20°N; %) relative to 1950–1999 mean in the historical (1860–2005) and RCP4.5 runs (2006–2300). Bottom right panel represents six-model means (black and orange lines) and their ±1σ (shading; Table 1). Whiskers at the bottom right indicate six-model means, 25%–75% ranges, and min-max ranges of ΔClt in 2070–2099 (green), 2170–2199 (yellow), and 2270–2299 (red), respectively.

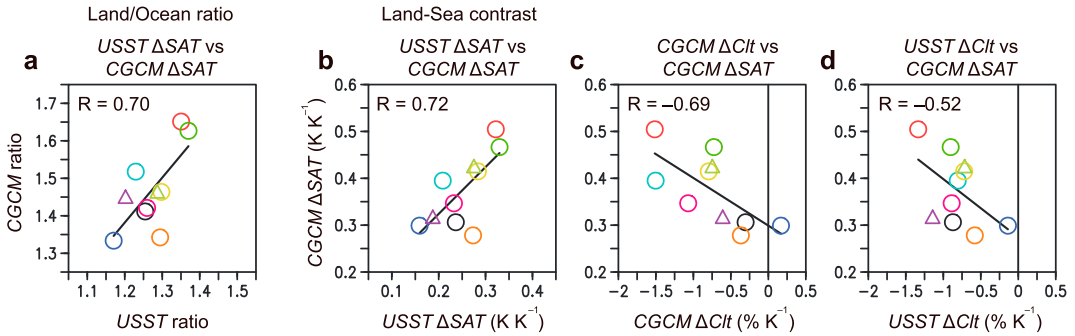

Figure 12. (a) Scatterplot of land to ocean warming ratio (K K^{-1}) over tropics (20°S–20°N) in USST and CGCM. (b) Similar to Figure 12a but for land-sea warming contrast (land minus ocean) normalized by ΔSATg (K K^{-1}). Land-sea ΔClt contrast over tropics normalized by ΔSATg (% K^{-1}) in (c) CGCM and (d) USST. *Y* axes in Figures 12c and 12d are identical to Figure 12b. Plotted marks are identical to Figure 10.

spread in the land to ocean warming ratio is informative when we consider the impacts of climate change because people live on land. In the last part of this paper, we examine the relationship between cloud feedback and the intermodel spread of the land warming amplification.

Figure 12 shows the relationship between relative ΔSAT over tropical land compared with ocean in USST and CGCM. Among the 10 models, the land to ocean warming ratio ranges from 1.33 to 1.65, consistent with the previous estimates [e.g., *Sutton et al*., 2007]. The relative warming ratios in CGCM correspond well with those in USST ($R = 0.70$), with a positive bias due to land warming associated with the fast response to radiative forcing (Figure 2). Land to ocean ΔSAT ratio in response to CO_2 increase and PAT-USST also shows intermodel spread [*Kamae et al*., 2014b], but the spread in USST dominates (49%). As for land-sea ΔSAT difference (land minus ocean), intermodel relationship (Figure 12b) is similar to the land/sea ratio (Figure 12a). Here land-sea ΔSAT contrasts are scaled by ΔSATg in the individual models.

Figure 12c shows the relationship between land-sea ΔClt contrast and ΔSAT contrast over the tropics in CGCM. Ten models clearly exhibit a negative correlation ($R = -0.69$), suggesting an effect of cloud feedback on the intermodel spread in the land-sea warming contrast. Among these models, negative correlation can also be found between USST and CGCM (Figure 12d). The land-sea ΔClt contrast in CGCM (Figure 12c) and USST (Figure 12d) can explain 47% and 27% of the intermodel spread of differential land warming in CGCM. This result suggests that the uncertainty in the cloud feedback found in USST is also important for that found in the CGCM simulations.

We should note that the intermodel correspondences could be sensitive to model ensembles and model number ($n = 10$) used here is limited although the relationship is statistically significant (at the 90% level of Student's *t* test). In addition, the cloud feedback is partly affected by the thermodynamic constraint (drying of the boundary layer and free troposphere), suggesting that the cloud reduction is also a result of anomalous land warming and drying driven by the differential thermodynamic properties between land and ocean. Although the SW cloud feedback plays an important role in the land-sea warming contrast [e.g., *Sejas et al*., 2014], the cloud change is not necessarily a trigger for the differential warming. More systematic frameworks are needed to quantify sources of the intermodel spread in the land warming amplification.

6. Summary and Discussion

We have quantified the dynamic and thermodynamic cloud feedbacks over tropical land by using ISCCP cloud radiative kernel and CMIP5 multimodels. The robust cloud reduction in the troposphere can be found over tropical land across CMIP5 models, resulting in a strong positive SW cloud amount feedback of 1.3 W m^{-2} K^{-1}. The cloud reduction corresponds to the tropospheric drying over land, indicating the importance of the thermodynamic cloud feedback. On the other hand, the land cloud reduction, the climatological atmospheric circulation, and its change show similar seasonal and regional variations. The MASC-induced weakening of large-scale atmospheric circulation over land results in a substantial dynamic cloud feedback that is largely comparable to the thermodynamic component. The thermodynamic constraints associated with the limited availability of water vapor over land and the dynamic cloud feedback are not sensitive to

the spatial pattern of SST change. Thus, the cloud reduction over tropical land in transient global warming simulations is largely associated with the global mean SST increase, resulting in the robust decreasing trend of cloud over tropical land.

Literatures examined the regionality and its uncertainty in the future precipitation change over the ocean [e.g., *Chou et al*., 2009; *Xie et al*., 2015]. The oceanic warming pattern that resulted from the atmosphere-ocean interactions [*Xie et al*., 2010] is a key factor for the uncertainty in the projected rainfall change [*Chadwick et al*., 2013; *Ma and Xie*, 2013; *Grose et al*., 2014; *Kent et al*., 2015]. Simple conceptual frameworks including "wet-get-wetter" and "warmer-get-wetter" are effective for better understanding of the regional uncertainty in the projected precipitation change over the ocean [*Huang et al*., 2013; *Watanabe et al*., 2014]. In addition, respective roles of the atmospheric circulation and water vapor content in the regional precipitation change and its uncertainty were examined from an atmospheric moisture budget perspective [*Seager et al*., 2010; *Long et al*., 2016]. However, these concepts cannot be applied simply to the land precipitation because of existence of inhomogeneous land surface properties including soil, land cover, land hydrology, orography, and human influences including aerosol emissions. Representations of mountains are not identical among different climate models, resulting in a source of uncertainty in the regional rainfall projections. The results of the current study suggest the relationship between the MASC mechanism and the dynamic reductions of cloud and precipitation over tropical land. However, the MASC mechanism is not sufficient to explain the land-sea contrasts in the changes in atmospheric circulation, cloud, and precipitation. Robustness and sources of uncertainty in the regional precipitation change over land should be quantified by systematic frameworks.

Acknowledgments

We thank three anonymous reviewers for their valuable comments on this manuscript. We acknowledge the scientific guidance of the World Climate Research Programme (WCRP) to promote this work, coordinated in the framework of WCRP Grand Challenge on Clouds, Circulation and Climate Sensitivity. We also thank the WCRP's Working Group on Coupled Modeling, which is responsible for CMIP, and we thank the climate modeling groups (listed in Table 1) for producing and making available their model output. For CMIP5, the U.S. Department of Energy's Program for Climate Model Diagnosis and Intercomparison provided coordinating support and led development of software infrastructure in partnership with the Global Organization for Earth System Science Portals. The authors thank S.-M. Long for helpful discussion. We appreciate M. Zelinka for providing the cloud radiative kernel. This work was supported by the Program for Risk Information on Climate Change (SOUSEI program) of the Ministry of Education, Culture, Sports, Science and Technology (MEXT), Japan. The CMIP5 data used in this study are available from the CMIP5 archive (http://cmip-pcmdi.llnl.gov/cmip5/). The code of cloud radiative kernel is available from the Cloud Feedback Model Intercomparison Project code repository (https://code.google.com/archive/p/cfmip-compute-cloud-feedbacks/).

References

Allen, M. R., and W. J. Ingram (2002), Constraints on future changes in climate and the hydrologic cycle, *Nature*, *419*, 224–232, doi:10.1038/nature01092.

Allen, R. J., J. R. Norris, and M. Kovilakam (2014), Influence of anthropogenic aerosols and the Pacific Decadal Oscillation on tropical belt width, *Nat. Geosci.*, *7*, 270–274, doi:10.1038/ngeo2091.

Anderson, B. T., B. R. Lintner, B. Langenbrunner, J. D. Neelin, E. Hawkins, and J. Syktus (2015), Sensitivity of terrestrial precipitation trends to the structural evolution of sea surface temperatures, *Geophys. Res. Lett.*, *42*, 1190–1196, doi:10.1002/2014GL062593.

Bayr, T., and D. Dommenget (2013), The tropospheric land–sea warming contrast as the driver of tropical sea level pressure changes, *J. Clim.*, *26*, 1387–1402, doi:10.1175/jcli-d-11-00731.1.

Blossey, P. N., C. S. Bretherton, M. Zhang, A. Cheng, S. Endo, T. Heus, Y. Liu, A. P. Lock, S. R. de Roode, and K.-M. Xu (2013), Marine low cloud sensitivity to an idealized climate change: The CGILS LES intercomparison, *J. Adv. Model. Earth Syst.*, *5*, 234–258, doi:10.1002/jame.20025.

Bony, S., and J.-L. Dufresne (2005), Marine boundary layer clouds at the heart of tropical cloud feedback uncertainties in climate models, *Geophys. Res. Lett.*, *32*, L20806, doi:10.1029/2005GL023851.

Bony, S., J.-L. Dufresne, H. LeTreut, J.-J. Morcrette, and C. Senior (2004), On dynamic and thermodynamic components of cloud changes, *Clim. Dyn.*, *22*, 71–86, doi:10.1007/s00382-003-0369-6.

Bony, S., G. Bellon, D. Klocke, S. Sherwood, S. Fermepin, and S. Denvil (2013), Robust direct effect of carbon dioxide on tropical circulation and regional precipitation, *Nat. Geosci.*, *6*, 447–451, doi:10.1038/ngeo1799.

Bretherton, C. S., P. N. Blossey, and C. Stan (2014), Cloud feedbacks on greenhouse warming in the superparameterized climate model SP-CCSM4, *J. Adv. Model. Earth Syst.*, *6*, 1185–1204, doi:10.1002/2014ms000355.

Brient, F., and S. Bony (2013), Interpretation of the positive low-cloud feedback predicted by a climate model under global warming, *Clim. Dyn.*, *40*, 2415–2431, doi:10.1007/s00382-011-1279-7.

Burke, M., S. M. Hsiang, and E. Miguel (2015), Global non-linear effect of temperature on economic production, *Nature*, *527*, 235–239, doi:10.1038/nature15725.

Ceppi, P., D. L. Hartmann, and M. J. Webb (2016), Mechanisms of the negative shortwave cloud feedback in middle to high latitudes, *J. Clim.*, *29*, 139–157, doi:10.1175/jcli-d-15-0327.1.

Chadwick, R., O. Boutle, and G. Martin (2013), Spatial patterns of precipitation change in CMIP5: Why the rich do not get richer in the tropics, *J. Clim.*, *26*, 3803–3822, doi:10.1175/jcli-d-12-00543.1.

Chadwick, R., P. Good, T. Andrews, and G. Martin (2014), Surface warming patterns drive tropical rainfall pattern responses to CO_2 forcing on all timescales, *Geophys. Res. Lett.*, *41*, 610–615, doi:10.1002/2013GL058504.

Chadwick, R., P. Good, G. Martin, and P. Rowell (2015), Large rainfall changes consistently projected over substantial areas of tropical land, *Nat. Clim. Change*, doi:10.1038/nclimate2805.

Chou, C., and D. J. Neelin (2004), Mechanisms of global warming impacts on regional tropical precipitation, *J. Clim.*, *17*, 2688–2701, doi:10.1175/1520-0442(2004)017<2688:MOGWIO>2.0.CO;2.

Chou, C., J. D. Neelin, C.-A. Chen, and J.-Y. Tu (2009), Evaluating the "rich-get-richer" mechanism in tropical precipitation change under global warming, *J. Clim.*, *22*, 1982–2005, doi:10.1175/2008jcli2471.1.

Dai, A. (2013), Increasing drought under global warming in observations and models, *Nat. Clim. Change*, *3*, 52–58, doi:10.1038/nclimate1633.

Dal Gesso, S., J. J. van der Dussen, A. P. Siebesma, S. R. de Roode, I. A. Boutle, Y. Kamae, R. Roehrig, and J. Vial (2015), A single-column model intercomparison on the stratocumulus representation in present-day and future climate, *J. Adv. Model. Earth Syst.*, *7*, 617–647, doi:10.1002/2014ms000377.

Demoto, S., M. Watanabe, and Y. Kamae (2013), Mechanism of tropical low-cloud response to surface warming using weather and climate simulations, *Geophys. Res. Lett.*, *40*, 2427–2432, doi:10.1002/grl.50474.

Deser, C., and A. S. Phillips (2009), Atmospheric circulation trends, 1950–2000: The relative roles of sea surface temperature forcing and direct atmospheric radiative forcing, *J. Clim.*, *22*, 396–413, doi:10.1175/2008jcli2453.1.

Dufresne, J.-L., and S. Bony (2008), An assessment of the primary sources of spread of global warming estimates from coupled atmosphere–ocean models, *J. Clim.*, *21*, 5135–5144, doi:10.1175/2008jcli2239.1.

Endo, H., and A. Kitoh (2014), Thermodynamic and dynamic effects on regional monsoon rainfall changes in a warmer climate, *Geophys. Res. Lett.*, *41*, 1704–1710, doi:10.1002/2013GL059158.
Fasullo, J. T. (2010), Robust land–ocean contrasts in energy and water cycle feedback, *J. Clim.*, *23*, 4677–4693, doi:10.1175/2010jcli3451.1.
Fasullo, J. T. (2012), A mechanism for land–ocean contrasts in global monsoon trends in a warming climate, *Clim. Dyn.*, *39*, 1137–1147, doi:10.1007/s00382-011-1270-3.
Feng, S., and Q. Fu (2013), Expansion of global drylands under a warming climate, *Atmos. Chem. Phys.*, *13*, 10,081–10,094, doi:10.5194/acp-13-10081-2013.
Flato, G. M., and G. J. Boer (2001), Warming asymmetry in climate change simulations, *Geophys. Res. Lett.*, *28*, 195–198, doi:10.1029/2000GL012121.
Garay, M. J., S. P. de Szoeke, and C. M. Moroney (2008), Comparison of marine stratocumulus cloud top heights in the southeastern Pacific retrieved from satellites with coincident ship-based observations, *J. Geophys. Res.*, *113*, D18204, doi:10.1029/2008JD009975.
Good, P., et al. (2015), Nonlinear regional warming with increasing CO_2 concentrations, *Nat. Clim. Change*, *5*, 138–142, doi:10.1038/nclimate2498.
Gregory, J. M., and J. F. B. Mitchell (1997), The climate response to CO_2 of the Hadley Centre coupled AOGCM with and without flux adjustment, *Geophys. Res. Lett.*, *24*, 1943–1946, doi:10.1029/97GL01930.
Grise, K. M., and L. M. Polvani (2014), The response of mid-latitude jets to increased CO_2: Distinguishing the roles of sea surface temperature and direct radiative forcing, *Geophys. Res. Lett.*, *41*, 6863–6871, doi:10.1002/2014GL061638.
Grose, M. R., J. Bhend, S. Narsey, A. Sen Gupta, and J. R. Brown (2014), Can we constrain CMIP5 rainfall projections in the tropical pacific based on surface warming patterns? *J. Clim.*, *27*, 9123–9138, doi:10.1175/jcli-d-14-00190.1.
Hartmann, D. L., et al. (2013), Observations: Atmosphere and surface, in *Climate Change 2013: The Physical Science Basis*, edited by T. F. Stocker, et al., pp. 159–254, Cambridge Univ. Press, Cambridge, U. K., and New York, doi:10.1017/cbo9781107415324.008.
He, J., and B. Soden (2015), Anthropogenic weakening of the tropical circulation: The relative roles of direct CO_2 forcing and sea surface temperature change, *J. Clim.*, *28*, 8728–8742, doi:10.1175/jcli-d-15-0205.1.
He, J., B. J. Soden, and B. Kirtman (2014), The robustness of the atmospheric circulation and precipitation response to future anthropogenic surface warming, *Geophys. Res. Lett.*, *41*, 2614–2622, doi:10.1002/2014GL059435.
Held, I. M., and B. J. Soden (2006), Robust responses of the hydrological cycle to global warming, *J. Clim.*, *19*, 5686–5699, doi:10.1175/jcli3990.1.
Huang, P. (2014), Regional response of annual-mean tropical rainfall to global warming, *Atmos. Sci. Lett.*, *15*, 103–109, doi:10.1002/asl2.475.
Huang, P., S.-P. Xie, K. M. Hu, G. Huang, and R. H. Huang (2013), Patterns of the seasonal response of tropical rainfall to global warming, *Nat. Geosci.*, *6*, 357–361, doi:10.1038/ngeo1792.
Intergovernmental Panel on Climate Change (2013), Summary for policymakers, in *Climate Change 2013: The Physical Science Basis*, edited by T. F. Stocker, et al., pp. 3–29, Cambridge Univ. Press, Cambridge, U. K., and New York, doi:10.1017/cbo9781107415324.004.
Joshi, M. M., J. M. Gregory, M. J. Webb, D. M. H. Sexton, and T. C. Johns (2008), Mechanisms for the land/sea warming contrast exhibited by simulations of climate change, *Clim. Dyn.*, *30*, 455–465, doi:10.1007/s00382-007-0306-1.
Kamae, Y., and M. Watanabe (2012), On the robustness of tropospheric adjustment in CMIP5 models, *Geophys. Res. Lett.*, *39*, L23808, doi:10.1029/2012GL054275.
Kamae, Y., and M. Watanabe (2013), Tropospheric adjustment to increasing CO_2: Its timescale and the role of land–sea contrast, *Clim. Dyn.*, *41*, 3007–3024, doi:10.1007/s00382-012-1555-1.
Kamae, Y., H. Shiogama, M. Watanabe, and M. Kimoto (2014a), Attributing the increase in Northern Hemisphere hot summers since the late 20th century, *Geophys. Res. Lett.*, *41*, 5192–5199, doi:10.1002/2014GL061062.
Kamae, Y., M. Watanabe, M. Kimoto, and H. Shiogama (2014b), Summertime land–sea thermal contrast and atmospheric circulation over East Asia in a warming climate–Part II: Importance of CO_2-induced continental warming, *Clim. Dyn.*, *43*, 2569–2583, doi:10.1007/s00382-014-2146-0.
Kamae, Y., M. Watanabe, T. Ogura, M. Yoshimori, and H. Shiogama (2015a), Rapid adjustments of cloud and hydrological cycle to increasing CO_2: A review, *Curr. Clim. Change Rep.*, *1*, 103–113, doi:10.1007/s40641-015-0007-5.
Kamae, Y., H. Shiogama, M. Watanabe, M. Ishii, H. Ueda, and M. Kimoto (2015b), Recent slowdown of tropical upper tropospheric warming associated with Pacific climate variability, *Geophys. Res. Lett.*, *42*, 2995–3003, doi:10.1002/2015GL063608.
Kent, C., R. Chadwick, and D. P. Rowell (2015), Understanding uncertainties in future projections of seasonal tropical precipitation, *J. Clim.*, *28*, 4390–4413, doi:10.1175/jcli-d-14-00613.1.
Kiehl, J. T., and V. Ramanathan (1990), Comparison of cloud forcing derived from the Earth Radiation Budget Experiment with that simulated by the NCAR Community Climate Model, *J. Geophys. Res.*, *95*(D8), 11,679–11,698, doi:10.1029/JD095id08p11679.
Klein, S. A., and C. Jakob (1999), Validation and sensitivities of frontal clouds simulated by the ECMWF model, *Mon. Weather Rev.*, *127*, 2514–2531, doi:10.1175/1520-0493(1999)127<2514:VASOFC>2.0.CO;2.
Knutti, R., and G. C. Hegerl (2008), The equilibrium sensitivity of the Earth's temperature to radiation changes, *Nat. Geosci.*, *1*, 735–743, doi:10.1038/ngeo337.
Knutti, R., and M. A. A. Rugenstein (2015), Feedbacks, climate sensitivity, and the limits of linear model, *Phil. Trans. R. Soc. A*, *373*, 20150146, doi:10.1098/rsta.2015.0146.
Li, W., L. Li, M. Ting, and Y. Liu (2012), Intensification of Northern Hemisphere subtropical highs in a warming climate, *Nat. Geosci.*, *5*, 830–834, doi:10.1038/ngeo1590.
Long, S., S.-P. Xie, and W. Liu (2016), Uncertainty in tropical rainfall projections: Atmospheric circulation effect and the ocean coupling, *J. Clim.*, doi:10.1175/jcli-d-15-0601.1.
Lu, J., G. A. Vecchi, and T. Reichler (2007), Expansion of the Hadley cell under global warming, *Geophys. Res. Lett.*, *34*, L06805, doi:10.1029/2006GL028443.
Ma, J., and S.-P. Xie (2013), Regional patterns of sea surface temperature change: A source of uncertainty in future projections of precipitation and atmospheric circulation, *J. Clim.*, *26*, 2482–2501, doi:10.1175/jcli-d-12-00283.1.
Ma, J., S.-P. Xie, and Y. Kosaka (2012), Mechanisms for tropical tropospheric circulation change in response to global warming, *J. Clim.*, *25*, 2979–2994, doi:10.1175/jcli-d-11-00048.1.
Manabe, S., and R. T. Wetherald (1975), The effects of doubling the CO_2 concentration on the climate of a general circulation model, *J. Atmos. Sci.*, *32*, 3–15, doi:10.1175/1520-0469(1975)032<0003:TEODTC>2.0.CO;2.
Manabe, S., R. J. Stouffer, M. J. Spelman, and K. Bryan (1991), Transient responses of a coupled ocean–atmosphere model to gradual changes of atmospheric CO_2. Part I: Annual mean response, *J. Clim.*, *4*, 785–818, doi:10.1175/1520-0442(1991)004<0785:TROACO>2.0.CO;2.
Meinshausen, M., et al. (2011), The RCP greenhouse gas concentrations and their extensions from 1765 to 2300, *Clim. Change*, *109*, 213–241, doi:10.1007/s10584-011-0156-z.
Mitchell, J., and W. Ingram (1992), Carbon dioxide and climate: Mechanisms of changes in cloud, *J. Clim.*, *5*, 5–21, doi:10.1175/1520-0442(1992)005<0005:CDACMO>2.0.CO;2.

Mizuta, R., O. Arakawa, T. Ose, S. Kusunoki, H. Endo, and A. Kitoh (2014), Classification of CMIP5 future climate responses by the tropical sea surface temperature changes, *SOLA*, *10*, 167–171, doi:10.2151/sola.2014-035.
Neelin, J. D., C. Chou, and H. Su (2003), Tropical drought regions in global warming and El Niño teleconnections, *Geophys. Res. Lett.*, *30*(24), 2275, doi:10.1029/2003GL018625.
O'Gorman, P. A., and C. J. Muller (2010), How closely do changes in surface and column water vapor follow Clausius–Clapeyron scaling in climate change simulations? *Environ. Res. Lett.*, *5*, 025207, doi:10.1088/1748-9326/5/2/025207.
Qu, X., A. Hall, S. A. Klein, and P. M. Caldwell (2015a), The strength of the tropical inversion and its response to climate change in 18 CMIP5 models, *Clim. Dyn.*, *45*, 375–396, doi:10.1007/s00382-014-2441-9.
Qu, X., A. Hall, S. A. Klein, and A. M. DeAngelis (2015b), Positive tropical marine low-cloud cover feedback inferred from cloud-controlling factors, *Geophys. Res. Lett.*, *42*, 7767–7775, doi:10.1002/2015GL065627.
Ringer, M. A., T. Andrews, and M. J. Webb (2014), Global-mean radiative feedbacks and forcing in atmosphere-only and coupled atmosphere–ocean climate change experiments, *Geophys. Res. Lett.*, *41*, 4035–4042, doi:10.1002/2014GL060347.
Seager, R., N. Naik, and G. A. Vecchi (2010), Thermodynamic and dynamic mechanisms for large-scale changes in the hydrological cycle in response to global warming, *J. Clim.*, *23*, 4651–4668, doi:10.1175/2010jcli3655.1.
Seidel, D. J., Q. Fu, W. J. Randel, and T. J. Reichler (2008), Widening of the tropical belt in a changing climate, *Nat. Geosci.*, *1*, 21–24, doi:10.1038/ngeo.2007.38.
Sejas, S. A., O. S. Albert, M. Cai, and Y. Deng (2014), Feedback attribution of the land-sea warming contrast in a global warming simulation of the NCAR CCSM4, *Environ. Res. Lett.*, *9*, 124005, doi:10.1088/1748-9326/9/12/124005.
Seneviratne, S. I., M. G. Donat, B. Mueller, and L. V. Alexander (2014), No pause in the increase of hot temperature extremes, *Nat. Clim. Change*, *4*, 161–163, doi:10.1038/nclimate2145.
Shaw, T. A., and A. Voigt (2015), Tug of war on summertime circulation between radiative forcing and sea surface warming, *Nat. Geosci.*, *8*, 560–566, doi:10.1038/ngeo2449.
Sherwood, S. C., S. Bony, and J.-L. Dufresne (2014), Spread in model climate sensitivity traced to atmospheric convective mixing, *Nature*, *505*, 37–42, doi:10.1038/nature12829.
Sherwood, S. C., S. Bony, O. Boucher, C. Bretherton, P. M. Forster, J. M. Gregory, and B. Stevens (2015), Adjustments in the forcing-feedback framework for understanding climate change, *Bull. Am. Meteorol. Soc.*, *96*, 217–228, doi:10.1175/bams-d-13-00167.1.
Sherwood, S., and Q. Fu (2014), A drier future? *Science*, *343*, 737–739, doi:10.1126/science.1247620.
Shiogama, H., S. Emori, N. Hanawaki, M. Abe, Y. Masutomi, K. Takahashi, and T. Nozawa (2011), Observational constraints indicate risk of drying in the Amazon basin, *Nat. Commun.*, *2*, 253, doi:10.1038/ncomms1252.
Soden, B. J., I. M. Held, R. Colman, K. M. Shell, J. T. Kiehl, and C. A. Shields (2008), Quantifying climate feedbacks using radiative kernels, *J. Clim.*, *21*, 3504–3520, doi:10.1175/2007jcli2110.1.
Sutton, R. T., B. Dong, and J. M. Gregory (2007), Land/sea warming ratio in response to climate change: IPCC AR4 model results and comparison with observations, *Geophys. Res. Lett.*, *34*, L02701, doi:10.1029/2006GL028164.
Taylor, K. E., R. J. Stouffer, and G. A. Meehl (2012), An overview of CMIP5 and the experiment design, *Bull. Am. Meteorol. Soc.*, *93*, 485–498, doi:10.1175/bams-d-11-00094.1.
Ueda, H., A. Iwai, K. Kuwako, and M. E. Hori (2006), Impact of anthropogenic forcing on the Asian summer monsoon as simulated by eight GCMs, *Geophys. Res. Lett.*, *33*, L06703, doi:10.1029/2005GL025336.
Vecchi, G. A., and B. J. Soden (2007), Global warming and the weakening of the tropical circulation, *J. Clim.*, *20*, 4316–4340, doi:10.1175/jcli4258.1.
Vial, J., J.-L. Dufresne, and S. Bony (2013), On the interpretation of inter-model spread in CMIP5 climate sensitivity estimates, *Clim. Dyn.*, *41*, 3339–3362, doi:10.1007/s00382-013-1725-9.
Watanabe, M., H. Shiogama, T. Yokohata, Y. Kamae, M. Yoshimori, T. Ogura, J. D. Annan, J. C. Hargreaves, S. Emori, and M. Kimoto (2012), Using a multi-physics ensemble for exploring diversity in cloud-shortwave feedback in GCMs, *J. Clim.*, *25*, 5416–5431, doi:10.1175/jcli-d-11-00564.1.
Watanabe, M., Y. Kamae, and M. Kimoto (2014), Robust increase of the equatorial Pacific rainfall and its variability in a warmed climate, *Geophys. Res. Lett.*, *41*, 3227–3232, doi:10.1002/2014GL059692.
Webb, M., C. Senior, S. Bony, and J. J. Morcrette (2001), Combining ERBE and ISCCP data to assess clouds in the Hadley Centre, ECMWF and LMD atmospheric climate models, *Clim. Dyn.*, *17*, 905–922, doi:10.1007/s0038201001.
Webb, M., et al. (2006), On the contribution of local feedback mechanisms to the range of climate sensitivity in two GCM ensembles, *Clim. Dyn.*, *27*, 17–38, doi:10.1007/s00382-006-0111-2.
Xie, S.-P., C. Deser, G. A. Vecchi, J. Ma, H. Y. Teng, and A. T. Wittenberg (2010), Global warming pattern formation: Sea surface temperature and rainfall, *J. Clim.*, *23*, 966–986, doi:10.1175/2009jcli3329.1.
Xie, S.-P., et al. (2015), Towards predictive understanding of regional climate change, *Nat. Clim. Change*, *5*, 921–930, doi:10.1038/nclimate2689.
Yin, J. H. (2005), A consistent poleward shift of the storm tracks in simulations of 21st century climate, *Geophys. Res. Lett.*, *32*, L18701, doi:10.1029/2005GL023684.
Zelinka, M. D., S. A. Klein, and D. L. Hartmann (2012a), Computing and partitioning cloud feedbacks using cloud property histograms. Part I: Cloud radiative kernels, *J. Clim.*, *25*, 3736–3754, doi:10.1175/jcli-d-11-00248.1.
Zelinka, M. D., S. A. Klein, and D. L. Hartmann (2012b), Computing and partitioning cloud feedbacks using cloud property histograms. Part II: Attribution to changes in cloud amount, altitude, and optical depth, *J. Clim.*, *25*, 3736–3754, doi:10.1175/jcli-d-11-00249.1.
Zelinka, M. D., S. Klein, K. Taylor, T. Andrews, M. Webb, J. Gregory, and P. Forster (2013), Contributions of different cloud types to feedbacks and rapid adjustments in CMIP5, *J. Clim.*, *26*, 5007–5027, doi:10.1175/jcli-d-12-00555.1.
Zhang, M., et al. (2013), CGILS: Results from the first phase of an international project to understand the physical mechanisms of low cloud feedbacks in single column models, *J. Adv. Model. Earth Syst.*, *5*, 826–842, doi:10.1002/2013ms000246.